Transport of surface states in the bulk quantum Hall effect

Sora Cho
Department of Physics, University of California, Santa Barbara, California 93106

Leon Balents
Institute for Theoretical Physics, University of California, Santa Barbara, California 93106

Matthew P. A. Fisher
Institute for Theoretical Physics, University of California, Santa Barbara, California 93106
and Department of Physics, University of California, Santa Barbara, California 93106
(Received 6 August 1997)

The two-dimensional surface of a coupled multilayer integer quantum Hall system consists of an anisotropic chiral metal. This unusual metal is characterized by ballistic motion transverse and diffusive motion parallel ($\hat{z}$) to the magnetic field. Employing a network model, we calculate numerically the phase coherent two-terminal z-axis conductance and its mesoscopic fluctuations. Quasi-one-dimensional localization effects are evident in the limit of many layers. We consider the role of inelastic dephasing effects in modifying the transport of the chiral surface sheath, discussing their importance in the recent experiments of Druist *et al.* [S0163-1829(97)04847-9]

I. INTRODUCTION

In a two-dimensional incompressible quantized Hall state, the low-energy excitations are confined to the edge of the sample. These edge states provide a simple way to understand transport in both integer and fractional quantum Hall systems.[1] For the integer quantum Hall effect with one filled Landau level, there is a single edge mode, describable in terms of a free chiral fermion. Edge states in the fractional quantum Hall effect (FQHE) are believed to be (chiral) Luttinger liquids, and have been probed via tunneling spectroscopy in several recent experiments.[2]

In recent years there has been much interest in multilayer quantum Hall systems. In double-layer systems the layer index plays the role of a pseudospin, and these systems have revealed a number of new surprises. In the opposite extreme with many layers, the samples become three dimensional, and a number of new features are expected. In such bulk samples with interlayer tunneling smaller than the Landau level spacing, the (integer) quantized Hall effect in each layer should survive, and the sample exhibit a $3d$ quantum Hall phase. Chalker and Dohmen[3] have recently discussed the phase diagram in such a system, in a model of noninteracting electrons with disorder. In the absence of disorder, the Landau levels will be broadened into bands in the presence of interlayer tunneling t. Disorder further broadens these bands. Near the band centers a diffusing three-dimensional (3D) metallic state is expected. In the tails of the Landau bands, the bulk states are localized, but current carrying edge states nevertheless lead to a quantum Hall effect. For one full Landau level, each layer has a single chiral free Fermion edge state, which together comprise a 2D subsystem—a chiral surface sheath.[3,4] This surface phase forms a novel 2D chiral metal system, which has been analyzed theoretically by a number of authors.[5–10] In the presence of impurity scattering, the transport is predicted to be very anisotropic, with ballistic in-plane motion and diffusive motion parallel to the magnetic field. Vertical transport in such a multilayer sample was first investigated experimentally in Ref. 11, and has recently been revisited by Druist *et al.*[12] The latter experiment provides striking evidence of the novel behavior characteristic of the chiral metal.

Most of the theoretical work on the chiral metal phase has focused on the mesoscopic regime, with the sample assumed smaller than the phase breaking lengths. The predicted behavior for such phase-coherent transport is very rich, with three different possible regimes (see Fig. 2) connected by universal crossovers.[4–6,8]

The purpose of this paper is twofold. First, we revisit the phase-coherent regime and study in detail the conductance and its fluctuations. Performing numerical transfer matrix calculations on a directed network model for the chiral metal enables us to extract the conductance and its fluctuations in the various regimes, and compare directly with earlier analytic approaches. We then address the important role of phase breaking processes, which have been ignored in earlier theoretical discussions.

The paper is organized as follows. In Sec. II we briefly review the existing theoretical predictions for the phase coherent transport. In Sec. III we describe the network model, and extract numerically the phase-coherent conductance in the various regimes. Section IV is devoted to a discussion of dephasing processes, and Sec. V to prospects and conclusions.

II. PHASE-COHERENT REGIME

For one full Landau level, there is a single free chiral Fermion edge mode in each layer, as depicted in Fig. 1. In the presence of an interlayer tunneling amplitude t (assumed much smaller than $\hbar\omega_c$), these chiral edge modes disperse along the z axis, and form one-half of an open 2D Fermi

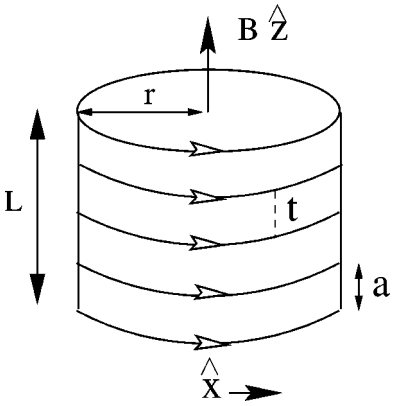

FIG. 1. Geometry of a multilayer quantum Hall system with an interlayer hopping amplitude t allowing vertical transport. With N layers the system has height $L=Na$, and a circumference $C=2\pi r$.

surface. Impurities cause electrons to scatter about the Fermi surface, as in any dirty metal. Due to the chiral nature, the in-plane motion remains ballistic with velocity v, even in the presence of impurities. However, the (interlayer) motion parallel to the field becomes diffusive, with diffusion constant D. Easier to measure than the ballistic velocity or diffusion constant is the z axis (2D sheet) conductivity σ_{zz} related to v and D via an Einstein relation[4]

$$\sigma_{zz}=e^2\rho D=\frac{D}{va}\frac{e^2}{h}, \tag{2.1}$$

where a is the interlayer (lattice) spacing and $\rho=1/hva$ the density of states. It will be convenient to introduce a dimensionless z-axis conductivity via $\sigma_{zz}=(e^2/h)\sigma$.

For a mesoscopic sample with finite circumference C and number of layers, $N=L/a$, there are several important time scales. For ballistic motion with velocity v, an electron circumnavigates the sample in a time $\tau_c=C/v$. In a time $\tau_L=L^2/D$ an electron will diffuse from the bottom to the top of the sample. The transport will be phase coherent provided the dephasing time τ_ϕ is much longer than both τ_c and τ_L. In principle, this mesoscopic regime exists for any sample at sufficiently low temperatures, since the dephasing time diverges as $T\to 0$ ($\tau_\phi\sim\hbar/k_BT$ in the quasi-one-dimensional limit of interest). Here we focus on the fully coherent regime, returning to dephasing effects in Sec. V.

For a sample with finite circumference C, there are two important length scales along the z axis, which demarcate the boundaries between three regimes (see Fig. 2).[4,5,8] Upon circumnavigating the sample once, an electron will diffuse along the z axis a distance $L_0=\sqrt{D\tau_c}$, which can be expressed in terms of the measurable z-axis conductivity σ as

$$L_0=(a\sigma C)^{1/2}. \tag{2.2}$$

For finite C with $L\to\infty$ the system is one dimensional, and localization along the z axis is expected. The (typical) localization length ξ for such a quasi-1D system is proportional to the (dimensionless) 1D conductivity, $\xi\sim\sigma_{1D}$, which can be written as

$$\xi=2\sigma C. \tag{2.3}$$

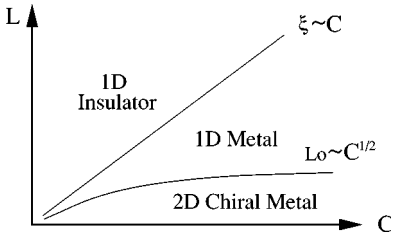

FIG. 2. Three different regimes of the phase-coherent transport of the surface sheath of a sample with height L and circumference C. Both L_0, the typical distance an electron diffuses along the z axis upon circling the sample once, and ξ, the 1D localization length, can be deduced from the measurable z-axis conductivity and geometrical parameters, as discussed in the text.

Thus both L_0 and ξ depend only on geometrical parameters, and the measurable z axis conductivity σ. Notice that $(\xi/a)=2(L_0/a)^2$, so that provided $L_0\gg a$ one has $\xi\gg L_0$.

As the height L of the sample varies, three regimes are possible (see Fig. 2). For $L<L_0\ll\xi$, an electron typically diffuses from the bottom to the top of the sample before circumnavigating the sample once. In this 2D *chiral metal* regime, an electron suffers dephasing in the leads before circling the sample. For $L_0\ll L\ll\xi$, the electron circles the sample many times, and phase-coherent processes around the sample are important. The system behaves like a phase-coherent *quasi-1D metal*. Finally, for $L\gg\xi$ 1D localization effects dominate, and the system is a *1D* (localized) *insulator*.

The predicted behavior for the phase-coherent z-axis conductance and its mesoscopic fluctuations depends sensitively on which regime the system is in. Consider first the (dimensionless) mean two-terminal conductance along the z axis, $\overline{G}$, where the overbar denotes an average over disorder realizations. In both the 2D chiral metal and the 1D metal regimes, Ohmic behavior is predicted with[8]

$$\overline{G}=\frac{C}{L}\sigma+O(L/\xi). \tag{2.4}$$

The usual ''weak localization'' corrections, which are of order $(L/\xi)^0$, are absent due to the breaking of time-reversal invariance. In the 1D insulating regime strong localization is operative, and the mean conductance is predicted to fall off exponentially with a universal form[13] (for $L\gg\xi$)

$$\overline{G}=2(\pi\xi/2L)^{3/2}\exp(-L/2\xi). \tag{2.5}$$

Conductance fluctuations are also of interest, which can be characterized by the variance, $\overline{\delta G^2}$, where $\delta G=G-\overline{G}$. In the 2D chiral metal and 1D metal regimes, Gruzberg, Read, and Sachdev[10] have shown that the variance can be written as

$$\overline{\delta G^2}=\Phi(L/L_0)+O(L/\xi), \tag{2.6}$$

where $\Phi(X)$ is a universal scaling function that smoothly connects the two regimes. Deep within the 1D metal regime the variance approaches a universal number well known for quasi-1D metals: $\Phi(L/L_0\to\infty)=1/15$. In the 2D chiral metal regime, $\Phi(L/L_0)\sim(L_0/L)^2$ for L/L_0 small. The conductance fluctuations are large in this limit, since the sample

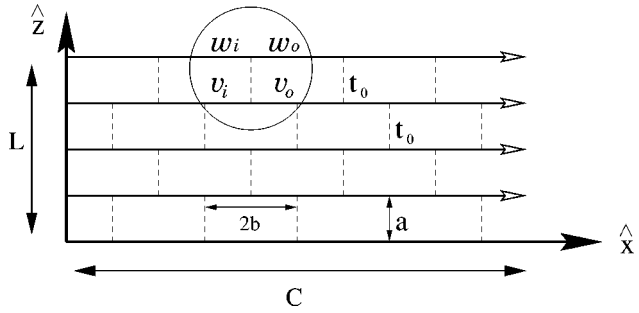

FIG. 3. Network model for the surface sheath. Here $N=L/a=4$ chiral edge modes are interconnected with dimensionless tunneling t_0, with periodic boundary conditions taken in the $\hat{x}$ direction of circumference C. The z-axis conductance is computed by employing a transfer matrix acting in the z direction.

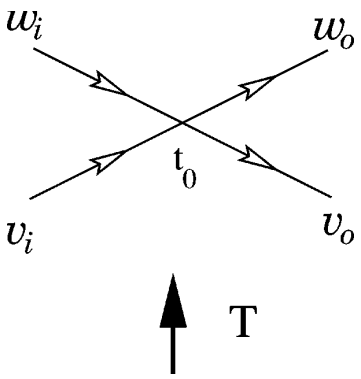

FIG. 4. The single node inside the circle in Fig. 3 (redrawn in a more conventional way) represented by the matrix in Eq. (3.3). The transfer matrix progresses from bottom to top.

effectively breaks up into $\tau_c/\tau_L=(L_0/L)^2$ incoherent regions, which add independently to the conductance and its fluctuations. Gruzberg, Read, and Sachdev[10] have obtained the full universal scaling function $\Phi(X)$, which interpolates between these two limits. In the 1D localized regime, the conductance is expected to be very broadly distributed, with an approximate log-normal distribution.

III. NUMERICS

A. Network model

Following Chalker and Dohmen,[3] we employ a simple network model to study phase-coherent transport of the surface sheath. The network model consists of directed links carrying electron current, connected via node parameters, as depicted in Fig. 3. All links carry current in the x direction, as appropriate for the chiral surface sheath. Scattering at the nodes is characterized by a (real and dimensionless) transmission amplitude t_0 for tunneling in the z direction between edge states in neighboring layers. For a given node the S matrix relating incoming to outgoing amplitudes is given explicitly by

$$\begin{pmatrix} w_{\rm out} \\ v_{\rm out} \end{pmatrix} = \begin{pmatrix} r_0 & t_0 \\ t_0 & -r_0 \end{pmatrix} \begin{pmatrix} w_{\rm in} \\ v_{\rm in} \end{pmatrix}, \tag{3.1}$$

with $t_0^2+r_0^2=1$. By construction, this matrix conserves the current, $|w_{\rm in}|^2+|v_{\rm in}|^2=|w_{\rm out}|^2+|v_{\rm out}|^2$. To model the disorder, the electrons are assumed to acquire a random phase along each link connecting adjacent nodes, taken for simplicity to be independent and uniformly distributed on the interval $[0,2\pi]$.

Periodic boundary conditions are taken in the ballistic x direction, with the circumference $C=2bN_c$, where b is the length of a single link in the x direction and N_c is the total number of interlayer tunneling nodes connecting adjacent edge modes (see Fig. 4). The network consists of N edge modes, with spacing a and a total ''height'' of $L=Na$.

The conductance along the z axis is obtained by computing the transmission of electrons from the bottom to the top of the sample. Specifically, we use the two-terminal Landauer formula to relate the (dimensionless) conductance G to the transmission matrix $\mathbf{t}$:[14]

$$G={\rm tr}[\mathbf{t}^+\mathbf{t}]. \tag{3.2}$$

The matrix elements t_{ij} are the amplitudes for an electron incident into channel (or node) i on the bottom edge to be transmitted into channel j on the top edge. Here N_c is the number of channels.

The transmission matrix is computed numerically by iterating a transfer matrix from the bottom to the top of the sample. This involves reexpressing each node in a form relating the amplitudes in one edge mode to the amplitudes in the adjacent edge mode:

$$\begin{pmatrix} w_{\rm in} \\ w_{\rm out} \end{pmatrix} = \begin{pmatrix} r_0/t_0 & 1/t_0 \\ 1/t_0 & r_0/t_0 \end{pmatrix} \begin{pmatrix} v_{\rm in} \\ v_{\rm out} \end{pmatrix}. \tag{3.3}$$

We study a range of system sizes with the channel number $N_c=4,8,16,32$ and the layer number $N=8,10,12,16$. Being interested in conductance fluctuations, it is necessary to evaluate the conductance exactly for each given disorder realization. The self-averaging Lyapunov exponents for a sample with $L\to\infty$ cannot be used to extract the sample to sample fluctuations in a finite system. This restriction imposes rather serious constraints on the accessible system sizes.

Since the microscopic parameters of the network model, t_0 and b, are not experimentally meaningful quantities, it is useful to relate them to a macroscopic observable, namely the measurable z-axis sheet conductivity of the surface sheath σ. As shown by Chalker and Dohmen,[3] this is possible for the network model, by summing the Feynman paths analytically. Specifically, consider paths that connect the incident electrons on the bottom edge to the transmitted electrons on the top edge. For $C\to\infty$ these paths do *not* fully circumnavigate the sample so that the interference between paths wrapping around the sample a different number of times—possible for finite C—is completely absent. In the absence of such interference the ensemble-averaged conductance reduces to a sum of classical probabilities: any two paths that pass through a different sequence of directed links will have a *random* relative phase, so that the interference term will vanish upon ensemble averaging. To sum the classical probabilities of these nonwinding paths we follow Chalker and Dohmen,[3] and consider the transmission probability for an electron incident in one channel (say i) to be transmitted through N layers: $T_N=\Sigma_j|t_{ij}|^2$. One can then ex-

press T_{N+1} in terms of T_N and the single-layer transmission probability, $T_1=t_0^2$, as a geometric sum:

$$T_{N+1}=\sum_{n=0}^{\infty} T_N(R_1R_N)^nT_1, \tag{3.4}$$

where $R_N=1-T_N$ is the reflection probability of N layers. Carrying out this geometric sum gives the recursion relation

$$\frac{1}{T_{N+1}}=\frac{1-T_1}{T_1}+\frac{1}{T_N}, \tag{3.5}$$

which can be readily solved for T_N. The average conductance in the absence of interference between paths winding around the sample is simply $\overline{G_0}=N_cT_N$, with N_c the number of channels. It is given exactly by

$$\overline{G_0}=\frac{N_c}{N}\frac{t_0^2}{1-t_0^2(1-1/N)}, \tag{3.6}$$

as obtained by Chalker and Dohmen[3] for $1/N\to\infty$. The z-axis sheet conductivity follows from Ohm's law, $\sigma=L\overline{G_0}/C$, which in the limit $C,L\to\infty$ becomes

$$\sigma=\frac{a}{2b}\frac{t_0^2}{1-t_0^2}. \tag{3.7}$$

Having related the conductivity to the network parameters, the mesoscopic crossover lengths L_0 and ξ for a *finite* size network model can be readily obtained from Eqs. (2.2) and (2.3).

The exact result for the conductance Eqs. (3.6) in the absence of interference between winding paths should be valid even for finite circumference, provided C is large enough so that winding paths are rare. The condition for the validity of ignoring the interference between winding paths is that $L\ll\sigma C\sim\xi$, so that the sample is in the 2D chiral metal or 1D metal regimes.

Notice that $\overline{G_0}$ in Eq. (3.6) is well defined even as $t_0\to1$. In this limit, the motion along the z axis also becomes ballistic (for finite N), and each channel is perfectly transmitted with $\overline{G_0}\to N_c$. It will be convenient to define an Ohmic conductance,

$$G_{\rm Ohm}\equiv C\sigma/L=\xi/2L, \tag{3.8}$$

which coincides with $\overline{G_0}$ when L is large enough that the z-axis motion is diffusive. As defined, $G_{\rm Ohm}$ diverges with σ as $t_0\to1$. The crossover from diffusive to ballistic z-axis motion occurs when $G_{\rm Ohm}\approx N_c$.

The 2D chiral metal regime requires that $L\ll L_0$, or equivalently $N\ll G_{\rm Ohm}$. However, to avoid a crossover into the ballistic regime of the network model requires $G_{\rm Ohm}<N_c$. Thus 2D chiral metal behavior is expected for $N\ll N_c$. Since this limit is difficult to access numerically, we focus below primarily on the 1D metallic and localized regimes.

B. Results

In Fig. 5 we show results for the ensemble-averaged two-terminal conductance $\overline{G}$ computed numerically from the network model, plotted versus the tunneling parameter t_0^2 for various channel numbers N_c at fixed height $N=12$. The solid lines are the ''classical'' conductance $\overline{G_0}$, Eq. (3.6), valid in the absence of interference between winding paths, and the dashed lines the ''Ohmic conductance,'' $G_{\rm Ohm}=C\sigma/L$. Notice that $\overline{G_0}$ gives a good fit to the numerical data, except in the low conductance regime, $\overline{G}<1$, where 1D localization effects are expected. The deviations from the classical behavior in this regime can be seen more easily in Fig. 6, where we plot the same data for the conductance, but now normalized by $\overline{G_0}$. Strong deviations are seen for small t_0^2, where the system enters into the 1D localized regime and interference between winding paths is critical.

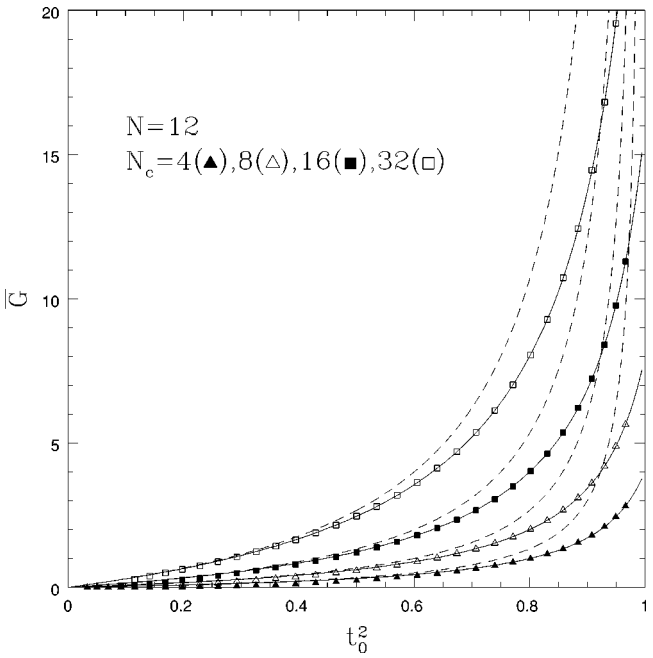

FIG. 5. The mean z-axis conductance $\overline{G}$ with fixed height $N=12$ for several different circumferences, plotted vs the dimensionless interlayer tunneling probability t_0^2. The solid lines are $\overline{G_0}$ given by Eq. (3.6), and the dashed lines are the Ohmic conductances $G_{\rm Ohm}=\xi/2L$ given in Eqs. (3.7) and (3.8).

In order to study the crossover from the 1D metallic to localized regime, we plot in Fig. 7 the mean conductance for $N=12$, normalized by $G_{\rm Ohm}=2\xi/L$, versus $2L/\xi$. The data show a crossover from a 1D metallic regime with Ohmic behavior, $\overline{G}\approx G_{\rm Ohm}$, to a 1D localized regime where the conductance vanishes exponentially for $L\gg\xi$. The solid line is the prediction from Mirlin, Muller-Groeling, and Zirnbauer[13] for the mean conductance of a quasi-1D metallic wire obtained using supersymmetry methods. The agreement is reasonable, but our numerics deviate from the universal form of Mirlin, Muller-Groeling, and Zirnbauer[13] at both large and small L/ξ. The deviations at large L/ξ are presumably due to lattice cutoff effects, since in this regime the localization length along the z axis is comparable to the network model lattice spacing a. The deviations for small L/ξ are probably due to finite-size effects. Indeed, as the channel number N_c increases, the agreement improves. Notice that $\overline{G}/G_{\rm Ohm}$ vanishes as $L/\xi\to0$ (rather than approaching unity)

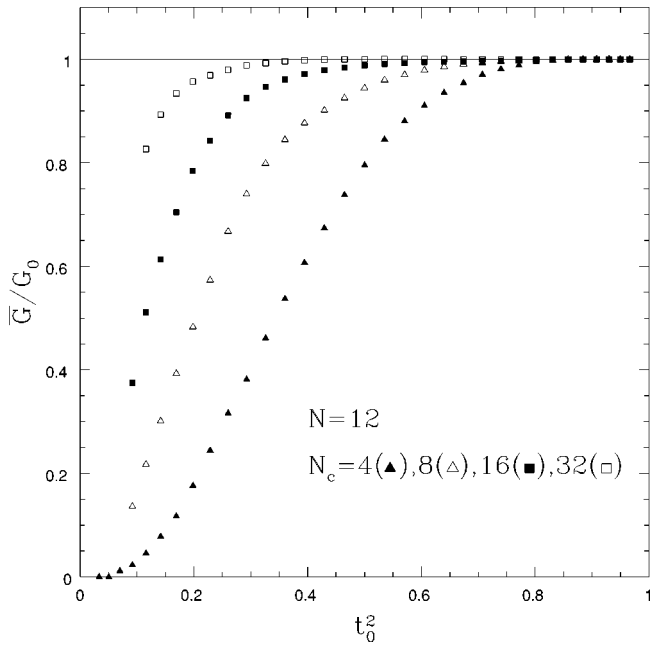

FIG. 6. The mean conductance $\overline{G}$ from Fig. 5 replotted after normalizing by G_0. The ratio $\overline{G}/G_0$ deviates from one as the system becomes localized.

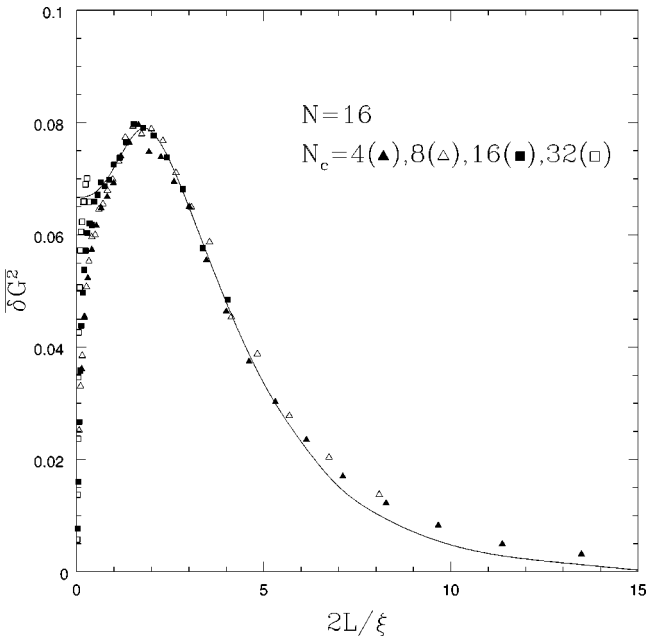

FIG. 8. Variance of the conductance for different sample sizes and hopping amplitudes t_0^2, all plotted vs $2L/\xi$. The solid line is the variance of the conductance for a quasi-1D sample, computed analytically by Mirlin, Muller-Groeling, and Zirnbauer.

due to ballistic behavior in the network model: in this limit $t_0 \to 1$ and $G_{\rm Ohm}$ diverges whereas $\overline{G}$ saturates at the (finite) channel number N_c.

In addition to the mean conductance, we have computed the sample-to-sample conductance fluctuations. In Fig. 8 we have plotted $\overline{\delta G^2}$ versus $2L/\xi$, for height $N=16$ and various different channel numbers. The solid curve is the universal prediction for the variance of the conductance of a quasi-1D wire, obtained by Mirlin, Muller-Groeling, and Zirnbauer.[13] This curve shows the crossover from the 1D metallic regime at small L/ξ, where the variance approaches the well-known universal value, $\overline{\delta G^2}=1/15$, to the 1D localized regime where the fluctuations vanish exponentially for $L \gg \xi$. The agreement between our numerical data and the Mirlin, Muller-Groeling, and Zirnbauer[13] theory is quite striking. Again, the deviations for $L/\xi \to 0$ are due to the ballistic regime in the network model for $t_0 \to 1$ (with finite N), where the conductance fluctuations vanish. For $L \gg \xi$ the localization length approaches the lattice spacing. The numerics and theory agree very well near the peak in the crossover regime.

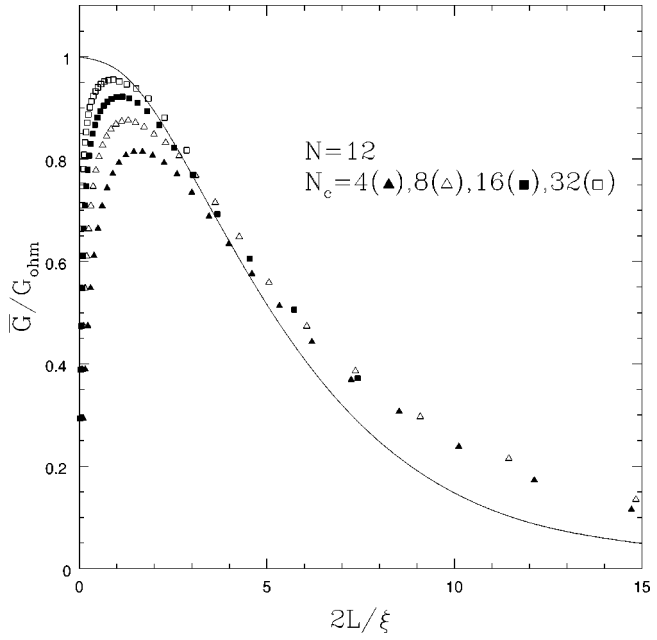

FIG. 7. The mean conductance normalized by $G_{\rm Ohm}=\xi/2L$ vs $2L/\xi$. For each sample size the points correspond to different values of the hopping probability t_0^2. The solid line is the mean conductance computed analytically for a quasi-1D system taken from paper of Mirlin, Muller-Groeling, and Zirnbauer.

Finally, we mention briefly our effort to extract numerically the conductance in the 2D chiral metal regime. This regime requires that $L \ll L_0$, or equivalently $N \ll G_{\rm Ohm}$. However, to avoid the ballistic regime when $t_0 \to 1$, we must require that $G_{\rm Ohm} < N_c$, so that we need $N \ll N_c$. We have focused on the conductance fluctuations in this regime, since these are predicted to behave very differently than in the 1D metal, diverging with $L/L_0 \to 0$ as $\overline{\delta G^2} \sim (L_0/L)^2$. In Fig. 9 the variance of the conductance is shown for ''short'' and ''wide'' samples, with height $N=8$ and width $N_c=16,32,64$, plotted versus L/L_0 where $L_0=\sqrt{a\sigma C}$. For each width N_c, we have varied the tunneling probability t_0^2 to get the set of data points. The solid line is the analytic prediction from Gruzberg, Read, and Sachdev[10] for the conductance variance in the crossover regime between the 1D and 2D chiral metal. Unfortunately, the agreement with the analytic result is quite poor, although the agreement improves for the widest sample with $N_c=64$. Indeed, the large enhancement in the variance for the sample with $N_c=64$ in the range $1<L/L_0<3$ is consistent with the theoretical expectations. The sharp drop in the conductance fluctuations for smaller L/L_0 is due to the

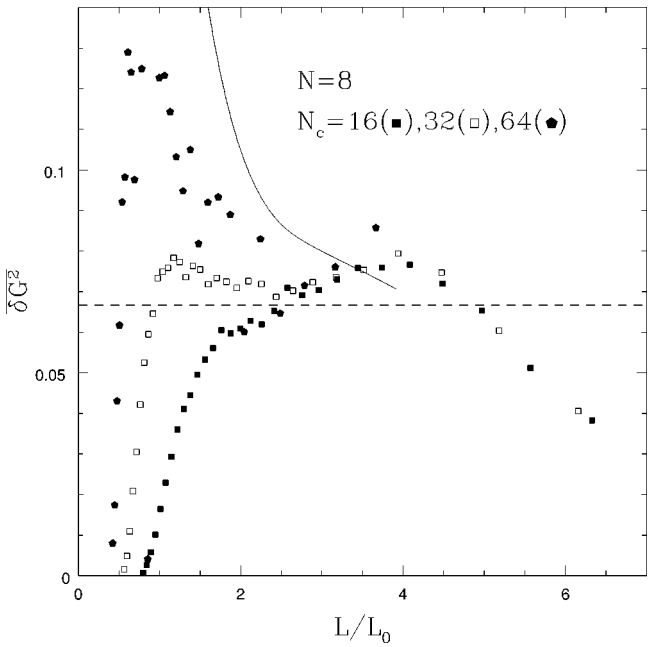

FIG. 9. Variance of the conductance vs L/L_0 for three different ''short'' and ''wide'' samples at various values of t_0^2. The solid line is the conductance variance computed analytically by Gruzberg, Read, and Sachder in the universal crossover regime between the 1D and 2D chiral metals. The dashed line is at $\overline{\delta G^2}=1/15$—the value in the 1D metal regime.

crossover from diffusive to ballistic motion in the network model. The local maxima for $N_c=16$ at $L/L_0\approx 4$ is the same maxima as in Fig. 8, and indicates a crossover into the 1D localized regime for larger L/L_0, where the Gruzberg, Read, and Sachdev results do not apply.

IV. INELASTIC EFFECTS

The above results for the phase coherent transport are dramatically modified in the presence of phase breaking effects. Dephasing effects can be characterized by a phase-breaking time, denoted τ_ϕ, which is the time an electron can propagate before having its phase randomized by interactions with other electrons or phonons. In the extreme anisotropic limit of the surface sheath with vanishing interlayer tunneling, $t=0$, an electron propagating in one edge state will interact via Coulomb forces with electrons in neighboring edges states, and can suffer phase-breaking inelastic scattering events. Being in 1D, the scattering rate, evaluated to leading order in the interactions strength u, is linear in temperature: $1/\tau_\phi=c(ul_B/2\pi\hbar v)^2 k_B T/\hbar$, with c an order one constant, l_B the magnetic length, and v the edge velocity. In practice, the dimensionless ratio $ul_B/\hbar v$ is itself also of order one, so that $1/\tau_\phi\sim k_B T/\hbar$. For nonzero but small interlayer tunneling, the dephasing rate will probably cross over to a two-dimensional T^2 dependence at very low temperatures.

Associated with the dephasing time are two dephasing lengths: (i) $l_\phi=v\tau_\phi$, the distance an electron propagates in the ballistic x direction before dephasing and (ii) $L_\phi=\sqrt{D\tau_\phi}=\sqrt{\sigma a l_\phi}$, the distance an electron diffuses parallel to the field in time τ_ϕ. Consider the transport geometry in Fig. 1, in which metallic contacts are applied at $z=0$ and $z=L$. For $L_\phi\gg L$, an electron diffuses between the two contacts before being dephased. In this case, transport is *mesoscopic*, and the above phase-coherent results apply.

For $L_\phi\ll L$, however, inelastic scattering occurs within the sample, and we must reconsider transport properties. There are two such important *incoherent* regimes, depending upon the relative magnitude of l_ϕ and C. For $l_\phi\ll C$, the electron does *not* fully circumnavigate the sample before suffering a phase-breaking collision. In this situation, electron paths that wind a different number of times around the sample do not interfere. As a result the system cannot explore the three phase *coherent* regimes discussed in Secs. II and III. Instead, the system is appropriately described as a phase-incoherent 2D chiral metal. Nevertheless, there are (small) mesoscopic fluctuations expected even in this limit, which we discuss below. In the opposite extreme of $l_\phi\gg C$, the electron can propagate many times around the sample before phase breaking. In this case, the one-dimensional motion parallel to the field is phase coherent up to a length scale L_ϕ. The system should behave like an incoherent quasi-1D wire, with L_ϕ the appropriate (1D) dephasing length, as we discuss further below.

To describe the transport behavior in these incoherent regimes, we employ arguments first applied in Ref. 15. The important observation is that the sample can be subdivided into ''patches,'' whose size is the maximum area over which an electron diffuses in time τ_ϕ. Each such region effectively acts as a classical resistor, and the whole sample then as a random resistor network, the properties of which are well understood.

First consider $l_\phi\ll C$. Then the patches have dimensions l_ϕ by L_ϕ, and form an array of size C/l_ϕ by L/L_ϕ. Denoting by g_i the (dimensionless) conductance (along the $z-$axis) of the ith patch, Ohm's law gives an average patch conductance of $\overline{g_i}=g_0=\sigma l_\phi/L_\phi$. The conductance fluctuations in each patch, $\delta g_i=g_i-g_0$, are of order one—being equivalent to the conductance fluctuations of a fully coherent network at the boundary between the 1D and 2D metal regimes. Since the mean conductance can be written as $g_0=L_\phi/a$, provided the patch size is larger than the lattice spacing, $L_\phi\gg a$, the conductance fluctuations in each patch are much smaller than the mean conductance: $\delta g_i\ll g_0$. In this limit, both the total conductance $\overline{G}$ and its variance, $\delta G^2=\overline{G^2}-(\overline{G})^2$, can be easily evaluated. A simple estimate is to imagine connecting the resistors (patches) only vertically (an approximation that gives the correct result for the conductance fluctuations up to an order one prefactor). Then for each column, the patch resistances add, so that $\delta G_{\rm col}^2\approx(L_\phi/L)^3$, which is independent of g_0. Contributing in parallel, the conductances of the $N_{\rm col}=C/l_\phi$ columns add, so that the variance of the *total* conductance is simply $\delta G^2=N_{\rm col}\delta G_{\rm col}^2$. This can be written in the form

$$\frac{\delta G^2}{\overline{G^2}}\approx\frac{a^2}{CL}\left[\frac{1}{\sigma}\frac{l_\phi}{a}\right]^{1/2}, \tag{4.1}$$

with $\overline{G}=C\sigma/L$. Notice that the conductance fluctuations have an appreciable temperature dependence entering

through l_ϕ, growing in magnitude at low temperatures. The mean conductance, however, remains temperature independent.

Consider next the 1D incoherent limit with $l_\phi \gg C$, in which the electron propagates many times around the sample before dephasing. In this limit, the L/L_ϕ classical patch resistors form a one-dimensional random chain, and have dimensions C by L_ϕ. Due to 1D localization effects, the conductance of each such segment will depend strongly on its length L_ϕ, and hence on the temperature T. For example, when L_ϕ is much smaller than the 1D localization length ξ, the (mean) conductance of each segment is given by

$$G_{\rm seg}(L_\phi) = (\sigma C/L_\phi) - \frac{2}{45}\frac{L_\phi}{\xi} + O(L_\phi/\xi)^2, \qquad (4.2)$$

where the first term is Ohm's law, and the second term reflects the leading 1D localization corrections within the unitary ensemble. In the opposite limit, $L_\phi \gg \xi$, one expects a stronger length (and temperature) dependence, $G_{\rm seg}(L_\phi) \sim \exp(-L_\phi/2\xi)$. The total conductance follows by simply adding the series resistances of each of the L/L_ϕ segments. In the 1D metallic regime with $L_\phi \ll \xi$, this gives

$$\overline{G} = \frac{\sigma C}{L} - \frac{2}{45}\frac{L_\phi}{L}\frac{L_\phi}{\xi} + \cdots, \qquad (4.3)$$

which depends on temperature through $L_\phi(T)$.

Experimentally, such conductance fluctuations are usually observed not by looking at different samples, but by varying the applied magnetic field in such a way as to change the phases accumulated by interfering electrons and thereby effectively change the disorder. The conductance fluctuations in this context are characterized not only by their amplitude, discussed above, but also by a characteristic field scale δB_ϕ. This scale is defined by the amount the applied field must be changed in order that the conductance of a fixed sample becomes uncorrelated with its previous value. Physically, the conductance fluctuations arise from constructive interference of two paths enclosing an area of the phase-coherent patch size. The total change in phase shift around this loop in units of 2π is simply the change in magnetic flux through this area divided by the flux quantum $\phi_0 = hc/e$. The characteristic field δB_ϕ, which changes the phase around the loop by $O(\pi)$, is thus simply the field that puts, say, half a flux quantum through this coherent area. Assuming the magnetic field has a non-negligible angle to the surface sheath (which we believe to be the case in the experiments of Druist *et al.*[12]), this gives

$$\delta B_\phi \approx \begin{cases} \phi_0/l_\phi L_\phi, & l_\phi \ll C \\ \phi_0/CL_\phi, & l_\phi \gg C \end{cases} \qquad (4.4)$$

in the two incoherent regimes. Note that since l_ϕ and L_ϕ increase as temperature is lowered, the conductance varies very rapidly with field at low temperatures.

V. CONCLUSIONS

We conclude with a comparison of these theoretical results to the experimental data of Druist *et al.*[12] Druist *et al.* have measured the z-axis transport in a series of multilayer quantum Hall samples. Specifically, the samples consisted of 50 layers of 150-Å GaAs layers alternating with 150 Å $Al_{0.1}Ga_{0.9}As$ barriers doped at their centers with silicon. The vertical separation between each of the 50 2D electron gases is $a = 300$ Å. A simple Kronig-Penney analysis gives an estimate for the z-axis bandwidth of $t = 0.12$ meV. When the applied magnetic field was tuned onto an integer quantum Hall plateau, the z-axis conductance—dropping with temperature—was found to saturate below about 200 mK. Since the low-temperature z-axis conductance scaled linearly with the circumference (perimeter) of the samples, which was in the range $400\ \mu{\rm m} \leq C \leq 7$ mm, Druist *et al.* argued that the conduction was being dominated by the 2D chiral surface sheath. The resulting sheet *conductivity* along the z axis was found to be $\sigma \approx 4 \times 10^{-4}$ on the $\nu = 1$ plateau, and about a factor of three larger for $\nu = 2$.

A theoretical estimate for the z-axis conductivity of the surface sheath at one full Landau level can be obtained from[4]

$$\sigma \approx \frac{a l_0}{\hbar^2 v^2} t^2, \qquad (5.1)$$

where l_0 is an elastic mean free path for edge scattering and v is the (ballistic) edge velocity. Unfortunately, both v and l_0 are difficult to estimate reliably, depending on the detailed slope and irregularities of the edge confining potential. However, we expect that in the limit of large magnetic field, $l_0 \gtrsim l_B$, where l_B is the magnetic length (l_0 may grow much longer than l_B as the edge is made cleaner). Moreover, we expect v to be bounded above by the edge velocity for a hard-wall confining potential, so that $v \lesssim \omega_c l_B/2\pi$, with ω_c the cyclotron frequency. Putting in these (rough) bounds, we obtain

$$\sigma \gtrsim \frac{(2\pi)^2 t^2 a}{\hbar^2 \omega_c^2 l_B}. \qquad (5.2)$$

Using the parameters appropriate for the Druist *et al.* experiment, this gives $\sigma \gtrsim 6 \times 10^{-5}$, about an order of magnitude smaller than the experimental value. Given the uncertainties in v and l_0, as well as possible shifts in t due to interaction effects, this level of agreement is reasonable.

Taking now the *measured* value of σ, we can estimate the two length scales that determine the system behavior in the mesoscopic limit. The samples studied by Druist *et al.* had a range of circumferences $400\ \mu{\rm m} \leq C \leq 7$ mm, which correspond to lengths $2 \leq L_0/a \leq 10$ and $10 \leq \xi/a \leq 200$, upon using Eqs. (2.2)–(2.3). Since $N = L/a = 50$ in these experiments, in the *mesoscopic* limit these samples should span the quasi-1D metal and 1D localized regimes. At low temperatures, we would therefore expect a strong suppression of the conductivity and significant temperature and circumference dependence, especially in the smaller samples. That such effects are not observed must be attributed to *inelastic* effects. Indeed, as shown below, estimates for the in-plane dephasing length l_ϕ give $l_\phi \ll C$ even at the lowest temperatures and for the smallest sample. In this limit, mesoscopic effects are greatly suppressed, and the system is best thought of as an *incoherent* 2D chiral metal. This accounts naturally for the observed low-temperature saturation of the conductivity [it

remains to be seen whether the weak residual temperature dependence at low T can be fitted to the expected[4] form $\sigma(T)-\sigma(0)\propto T^2$].

We can attempt to estimate the dephasing length l_ϕ via

$$l_\phi = A\left(\frac{hv}{ul_B}\right)^2 \frac{hv}{k_B T}, \tag{5.3}$$

however, there is considerable uncertainty in the parameters—particularly the edge velocity v. As a crude estimate we take $A=1$, a dimensionless interaction strength of unity $ul_B/hv=1$ and an edge velocity estimated for a hard-wall confining potential $v=\omega_c l_B/2\pi$. In the 10 T field used by Druist *et al.* in the $\nu=1$ plateau and at the lowest temperatures studied of $T=50$ mK this gives the rough estimate $l_\phi \sim 20$ μm.

Fortunately, one can also extract estimates for l_ϕ directly from the experimentally measured conductance fluctuations. In fact, this can be done in two ways, thereby providing a consistency check. One determination is from the *amplitude* of the fluctuations. Solving Eq. (4.1) gives

$$l_\phi \approx \tilde{A}\frac{CN^3}{\overline{G^3}}(\delta G^2)^2. \tag{5.4}$$

Because the fourth power of δG appears above and the amplitude $\tilde{A}$ is unknown, there is again considerable uncertainty in l_ϕ. For the Druist *et al.* experiments, we obtain $l_\phi \approx 26$ μm, consistent with the above theoretical estimate.

A second determination comes from the magnetic field scale of the conductance fluctuations. From the above estimates, we see that $L_\phi=\sqrt{\sigma a l_\phi} \lesssim a$ (using the measured $\sigma=4\times10^{-4}$). This is close to the ''incoherent tunneling'' limit, and we expect it is appropriate to replace $L_\phi \to a$ in Eq. (4.4), giving

$$l_\phi \approx \frac{\phi_0}{a\,\delta B_\phi}. \tag{5.5}$$

For the Druist *et al.* experiment, this gives $l_\phi \approx 3$ μm at $T=100$ mK, somewhat smaller than the first estimate. In this case there are also considerable uncertainties due primarily to incomplete knowledge of the degree of interlayer flux penetration. However, all three of the above estimates give $l_\phi \ll C$.

In summary, the experiments so far are consistent with the picture of an *incoherent 2D chiral metal*. Several opportunities exist for further theoretical and experimental study. Samples with smaller circumferences in the range of 10–20 μm would be highly desirable, since the mesoscopic regime would then be accessible below several hundred mK. In this limit, the rich and varied crossovers between the three mesoscopic regimes could be accessed experimentally. Theoretically, a more quantitative study of inelastic scattering and dephasing lengths would be desirable in order to achieve a precise comparison with experiment. Particularly interesting from both points of view is the temperature dependence of $1/\tau_\phi$, which we believe should exhibit linear scaling with temperature over a broad range. A field-theoretic treatment of dephasing effects could be useful in providing the desired tighter link with experiments.

ACKNOWLEDGMENTS

We thank David Druist and Elizabeth Gwinn for generously sharing their experimental data. It is a pleasure to acknowledge fruitful conversations with Ilya A. Gruzberg, Nick Read, and Hsiu-Hau Lin. We are grateful to the National Science Foundation for support, under Grant No. PHY94-07194, DMR-9400142, and DMR-9528578.

[1] For a general discussion of edge state transport, see C.L. Kane and M.P.A. Fisher, in *Perspectives in the Quantum Hall Effect*, edited by S. Das Sarma and A. Pinczuk (Wiley, New York, 1997), and references therein.

[2] F.P. Milliken, C.P. Umbach, and R.A. Webb, Solid State Commun. **97**, 309 (1996): A.M. Chang, L.N. Pfeiffer, and K.W. West, Phys. Rev. Lett. **77**, 2538 (1996); P.J. Turley, D.P. Druist, E.G. Gwinn, K. Maranowski, K. Campmann, and A.C. Gossard (unpublished).

[3] J.T. Chalker and A. Dohmen, Phys. Rev. Lett. **75**, 4496 (1995).

[4] L. Balents and M.P.A. Fisher, Phys. Rev. Lett. **76**, 2782 (1996).

[5] H. Mathur, Phys. Rev. Lett. **78**, 2429 (1997).

[6] L. Balents, M.P.A. Fisher, and M.R. Zirnbauer, Nucl. Phys. **B483**, 601 (1996).

[7] Y.-K. Yu, cond-mat/9611137 (unpublished).

[8] I.A. Gruzberg, N. Read, and S. Sachdev, Phys. Rev. B **55**, 10 593 (1997).

[9] Y.B. Kim, Phys. Rev. B **53**, 16 420 (1996).

[10] I.A. Gruzberg, N. Read, and S. Sachdev, cond-mat/9704032 (unpublished).

[11] H.L. Stormer *et al.*, Phys. Rev. Lett. **56**, 85 (1986).

[12] D.P. Druist, P.J. Turley, and E.G. Gwinn (unpublished).

[13] A.D. Mirlin, A. Muller-Groeling, and M.R. Zirnbauer, Ann. Phys. (N.Y.) **236**, 325 (1994).

[14] D.S. Fisher and P.A. Lee, Phys. Rev. B **23**, 6851 (1981).

[15] A. Miller and E. Abrahams, Phys. Rev. **120**, 745 (1960).